Available online at https://link.springer.com/journal/42241
http://www.jhydrodynamics.com
Journal of Hydrodynamics, 2022
https://doi.org/10.1007/s42241-023-0087-y

An overview of flow field computational methods for hydrodynamic noise prediction

Wei-wen Zhao[1], Zhi Pan[2], Lian-jie Yu[1], De-cheng Wan[1*]
1. *Computational Marine Hydrodynamics Lab (CMHL), School of Naval Architecture, Ocean and Civil Engineering, Shanghai Jiao Tong University, Shanghai 200240, China*
2. *Wuhan Second Ship Design and Research Institute, Wuhan 430205, China*

(Received December 18, 2022, Revised December 21, 2022, Accepted December 22, 2022, Published online January 12, 2023)

Abstract: Recently, the hydrodynamic noise is becoming a research hotspot because it not only affects the concealment and comfort of ships, but also affects the living condition of underwater mammals. Accurate prediction of hydrodynamic noise requires that the detailed flow field has been simulated temporally and spatially with high fidelity method. In this paper, we introduce the current issues and challenges for the prediction of hydrodynamic noise, and provide an overview to several detailed flow field simulation methods which aim to resolve these issues. The overview could point the future directions for hydrodynamic noise prediction.

Key words: Hydrodynamic noise, turbulent fluctuation, wall-bounded flow, two-phase flow, noise reduction

Introduction

The hydrodynamic noise, or hydroacoustics, refers to the sounds that occur in the ocean, is an important issue and has drawn much attention of researchers and scientists recently. The sounds can come from a variety of sources, such as marine structures, earthquakes and marine animals. Those generated from marine structures is the main part of hydrodynamic noise. The hydrodynamic noise not only affects the concealment and comfort of ships, but also has a negative impact on marine life. As a result, understanding and managing noise is essential for both scientific and engineering research purposes.

Conventionally, the prediction for acoustics can be classified into two groups of methods. The first one is the direct method in which the generation and propagation are directly computed by solving the flow governing equations. However, this method is impractical for complex engineering flows due to that the acoustic scales are at least a magnitude smaller than the flow scales and thus very fine computational mesh is required[1]. Furthermore, the computational cost is unaffordable for far field (e.g., hundreds of lengths away from a ship) sound prediction. It is also worth noting that this approach is not suitable for hydrodynamic noise due to the conflict between the incompressible characteristics of the flow field and the compressibility of the sound field. The second one is the hybrid method in which the generation and propagation of sound are decoupled and solved separately. The generation of sound is computed by solving the near field flow region though classical computational fluid dynamics (CFD) simulations, and the far field radiation and propagation is solved through acoustic analogies.

In this overview, several flow field computational methods are selected with a focus on the requirement of hydrodynamic noise. A brief introduction of each section is given as follows. Section 1 introduces some flow field simulation methods for underwater acoustics without free-surface. In Section 2 the free-surface is taken into consideration and special treatments for modeling two-phase flow are presented. Section 3 reviewed some research progresses for reduce hydrodynamic noises. In Section 4 the conclusions and outlook are presented.

Project supported by the National Natural Science Foundation of China (Grant Nos. 51909160, 52131102), the National Key Research and Development Program of China (2022YFC2806705, 2019YFB1704200).
Biography: Wei-wen Zhao (1990-), Male, Ph. D.,
E-mail: weiwen.zhao@sjtu.edu.cn
Corresponding author: De-cheng Wan,
E-mail: dcwan@sjtu.edu.cn

1. Single-phase flow without interface

For acoustic prediction of single-phase flow, the most commonly used analogy methods are based on the Ffowcs Williams and Hawkings (FW-H) formulation[2]. The FW-H formulation constructs a sound propagation equation with equivalent acoustic sources such as monopole, dipole, and quadrupole. The monopole and dipole sources are linear and computed over a solid or permeable control surface, and the quadrupole sources are nonlinear and computed over the volume outside of the control surface.

1.1 *Wall-bounded turbulent flow prediction*

In most cases, the hydrodynamic noises are caused by the interaction between flows and objects. The fluctuations inside turbulent boundary layer are vital for accurate computation of sound generation. For linear sound sources, the permeable control surface does not usually match the actual solid surface of the object. But it should envelop all the surfaces in the flow as well as the most turbulent regions.

Previous studies used direct numerical simulation (DNS)[3] and wall-resolved large-eddy simulation (WRLES)[4-5] coupled with FW-H formulation to predict acoustics. However, DNS and WRLES are computationally expensive and are limited to low Reynolds number flows. According to the CFD vision by NASA[6], WRLES for engineering flows will still be hardly affordable and out of reach even with 2030 leading high performance computing machines. The challenge of using WRLES for wall-bounded turbulent flows comes from the decrease of turbulent length scale when approaching the solid wall. Previous study by Larsson et al.[7] has showed that the grid points required for resolving inner viscous sublayer are at the order of $Re^{2.16}$, and the grid point for outer layer scales with $Re^{0.58}$. As a result, up to 90% of the grid points in the boundary layer are used for the viscous sublayer, which only makes up to 10% of the boundary layer thickness.

This observation has led to the development of wall-modeled LES (WMLES) which can significantly reduce the grid resolution requirements near solid walls. The WMLES utilizes fine grid at the outer portion of boundary layer to resolve the energy-containing eddies. While it models the effects of near-wall velocity with a reasonable stress model. In this regard, the WMLES not only removes the prohibitive WRLES grid requirements for inner boundary layer, but also decreases the total number of time steps since the time step is usually determined by the smallest grid size.

The basic idea of WMLES is to construct a wall model which computes the shear stress near wall. The modeled shear stress will then be exposed as a boundary condition to the LES solver for solving the outer portion of the boundary layer and other resolved flow regions. Depending on the types of solved equations in the inner boundary regions, wall models can be divided into non-equilibrium and equilibrium types. Non-equilibrium wall models are based on the 3-D RANS equations. In most cases, the 3-D RANS equations are simplified to the thin boundary layer equations (TBLE) for solving the wall-parallel velocity components. For non-equilibrium wall models, the TBLE are a set of partial differential equations that retains all or part of the temporal, convection and pressure gradient terms. By solving the TBLE, non-equilibrium wall models can capture the unsteady and non-equilibrium characteristics such as flow separation and vortex shedding. Suga et al.[8] proposed an algebraic non-equilibrium wall-stress model. The wall-stress model was coupled with the standard Smagorinsky model and applied to the simulation of turbulent channel flows and backward-facing step flow. Results showed that the algebraic model is better and less grid sensitive than the traditional equilibrium wall-stress model. Lozano-Durán et al.[9] proposed a model that captures the response of non-equilibrium wall-bounded turbulence under the imposition of 3-D strain and assessed the ability of the state-of-the-art wall-modelled large-eddy simulation to predict non-equilibrium 3-D flows.

Equilibrium wall models assume that the local flow is equilibrium, which implies that the local flow characteristics in the transport of a quantity near a wall are dominated by the turbulent dissipation process. With this assumption, the RANS equations are reduced to a set of ordinary differential equations by discarding the temporal, convection and pressure gradient terms. Iyer and Malik[10] performed a priori and a posteriori analyses of the equilibrium wall model for high-speed wall-bounded turbulent flows. They tested and discussed the effects of different mixing-length-based eddy-viscosity models and damping functions. Mehrabadi and Bodony[11] examined the capability of equilibrium WMLES approach together with the Prandtl's mixing length model and van Driest damping function for predicting the broadband noise generated by a NACA 0012 airfoil. They found out that the WMLES can provide a good prediction of the skin friction coefficient for different grid resolutions. However, other quantities, such as the mean velocity profile, are sensitive to the grid resolution. Boukharfane et al.[12] applied an equilibrium WMLES to predict the flow of air passing a controlled-diffusion blade and to study the blade broadband noise that is generated from the interaction of turbulent boundary layer with a lifting surface trailing edge. They showed that WMLES accurately predicts the mean pressure coefficient distribution, velocity statistics (including the mean velocity), and

the traces of Reynolds tensor components. In addition, the predicted instantaneous flow structures resemble those found in the reference WMLES database.

Overall, the WMLES is suitable for the acoustic prediction for industrial flows. For turbulent flows with complex geometries, the non-equilibrium wall models theoretically perform better than equilibrium wall models because they account for unsteady flow characteristics by considering the temporal, convection and pressure gradient term. But validations for WMLES on predicting flow separation and vortex shedding in practical engineering applications with complex geometries are still needed.

1.2 *High-order discretization scheme*

In FW-H formulation, the quadrupole term which represents the nonlinear effects is often ignored in aeroacoustics. However, recent hydroacoustic studies have shown that the influence of nonlinear terms can be significant[13]. The nonlinear quadrupole term should be integrated over a volume region outside of the control surface. The flow information such as pressure and velocity and their spatial derivatives in the volume region are required for computing nonlinear term. When dealing with turbulent flows with unsteady characteristics, the high-order schemes are preferred to discretize the space in order to avoid numerical dissipation and obtain high fidelity sound sources generated by unsteady flows.

Among the variety of spatial discretization methods, the most popular three are the finite difference (FD) method which performs discretization of governing equations on structured grid, the finite volume (FV) method which decomposes the domain into a finite set of cells and solves governing equations after cell volume integration, the finite element method which utilizes a polynomial to approximate the distribution of unknowns. For FD methods, high-order can be achieved by simply expanding the cell stencils. High-order FV methods are non-trivial compared with FD methods. One of the most popular high-order FV methods are the essentially non-oscillatory (ENO) and weighted ENO (WENO)[14] schemes which include a local polynomial reconstruction to increase the spatial approximation accuracy and reduce the numerical diffusion. For FE methods, the high-order schemes can be constructed by increasing the degrees of the polynomials. The discontinuous Galerkin (DG)[15] are one of the most commonly used high-order FE methods. The solution of DG does not necessary to be continuous. It introduces the flux computation between adjacent element to allow the coupling between discontinuous cells. Beside the above, there are some other high-order method families such as the spectral element (SE)[16] and the flux reconstruction (FR)[17-18]. For all of the high-order methods, the main efforts are made to avoid numerical oscillations and improve solution accuracy and robustness.

In recent years, high-order schemes have been applied for acoustic predictions. Marino et al.[19] employed implicit LES with high order DG spectral element scheme to compute the aeroacoustics generated by a 3-D wind turbine airfoil. The noise generated by direct computations and the FW-H formulation were compared and good agreement for both models was found for the far field noise, except some discrepancies at high frequency range. Alhawwary and Wang[20] coupled high-order FR method with a generalized FW-H acoustic analogy for moving medium problems. The implementation was validated against a supersonic jet and an idealized generic side mirror. The computed near- and far-field noise spectra were in good agreement with experimental measurement. Shen and Miller[21] also utilized LES based on high-order FR scheme for supersonic jet simulation and consequently used FW-H for far-field acoustic prediction.

1.3 *Dynamic mesh with moving body*

To predict hydroacoustics of moving bodies with complex motions, the dynamic overset grid method is preferred. In addition, the detailed flow field around the moving bodies should be computed accurately which involves the adaptive mesh refinement.

The dynamic overset method is well suited for solving problems involving large translations and rotations of rigid bodies. For example, for the problem of ship maneuvering on waves, the overset grid technology considers the large-scale motion of the ship on the waves, as well as the complex relative motion between the ship, propeller and rudder[22]. Its basic idea is to generate grids for each moving object, and then combine and superimpose these grids to form a whole mesh. Each grid moves independently, and the interpolation is performed to transform information between different grids. The overset technology is a modular method essentially, which avoids excessive distortion of mesh due to the object motion. In addition, overset method can replace any grid in the system easily, realizing the rapid replacement of different parts.

Overset grids have been widely used in the field of ship and ocean engineering. For example, Carrica et al.[23] used the overset solver “CFDShip-Iowa” to simulate the zig-zag maneuvering motion of the KCS ship in shallow water numerically. Shen[24-26] integrated the commercial overset assembly library Suggar++[27] into the open source framework OpenFOAM, and developed the solver “naoe-FOAM-SJTU” which is suitable for ship hydrodynamic problems. Based on the solver, Wang et al.[28] carried out self-propulsion test of ONR Tumblehome (ONRT) ship model with fully attached double propellers and

rudders. The ability of the "naoe-FOAM-SJTU" solver to solve the ship maneuvering problem is verified. Figure 1 shows a typical assembled overset grid system for the ship hull-propeller-rudder system.

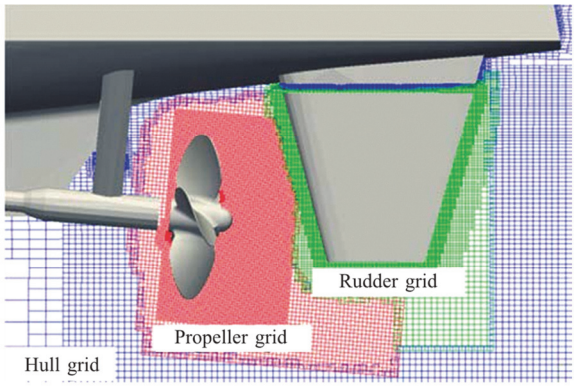

Fig. 1 (Color online) Overset grid distribution for ship hull[29]

Previous study has showed that the hydroacoustic results are sensitive to grid resolution[30]. There is a need to improve grid resolution in order to get accurate hydroacoustic performance. One common approach is to refine grid at the regions around the trajectory of the moving object. However, this will increase the grid points vastly and is not efficient for computation. Another alternative is the adaptive mesh refinement (AMR) technology which aims to improve the grid resolution of local areas by changing the grid topology and increasing the number of local grids on the basis of static grids, thereby improving the accuracy of local simulations significantly. In common case, the grid is split in the form of a multi-tree to increase the total amount of local grids. The multi-tree technique means that the existing grid is used as parent node, and the child nodes are split from it as a new grid for adaptive refinements, as shown in Fig. 2.

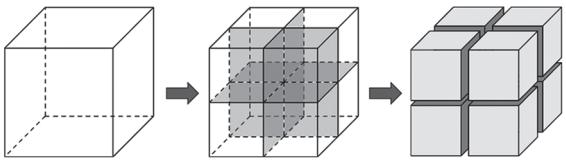

Fig. 2 Adaptive refinement for 3-D Mesh

In order to refine the grid, a criterion should be determined. A refinement parameter and its threshold are required in adaptive mesh refinement procedure, and all cells which satisfy the specified threshold are the candidates to be refined in the current time step. If the grid that has not been refined at the previous time step are selected as the object at current time step, the number of grids in this area will increase. Otherwise, the number of grids in this area will be reduced. Therefore, at each time step, the two aspects of splitting and deleting child nodes are carried out at the same time.

Based on the OpenFOAM platform, Wang et al.[31] applied AMR to study the cavitation flow around a rotating body. The results show that increasing the adaptive refinement level can improve the numerical simulation significantly without increasing the computational cost greatly. Lidtke et al.[32] used AMR to simulate propeller tip vortex cavitation, and the results showed that the details of tip vortex are presented better. Ku et al.[33] applied AMR method to study the tip vortex cavitation noise of underwater submarine propellers. The acoustic radiation was obtained by solving the FW-H equation. The predicted hydroacoustic pressure spectra due to the propellers' cavitating flow show good agreements with the measured ones. Sezen and Atlar[34] investigated the hydroacoustic performance of the INSEAN E779A propeller with coupled detached-eddy simulation (DES) and permeable FW-H formulation. The flow field was computed by a vorticity-based AMR method and the numerical results were validated with the sea trial data.

2. Two-phase flow with air-water interface

The free surface flows with air-water interface are commonly encountered in ship and ocean engineering. It is an important source of noise, especially free surface noise, cavitation noise and air-water-bubble mixed flow noise. Compared with single-phase flow noises, the two-phase flow noises have more complex sound sources and propagation model.

2.1 *Free surface capturing*

To consider free surface effect on hydroacoustics, the hybrid method of coupling CFD and acoustic analogy is a common approach. There are mainly two aspects with is approach: the accurate modelling of free surface flow in CFD and the accurate modelling of free surface reflection in acoustic analogy.

The volume of fluid (VOF) is the most commonly used method for free surface flow. The basic idea of VOF method is to define a volume fraction f on each cell, which is determined by the volume fraction of water or gas in this cell element[35]. VOF methods can be classified into two categories. One is geometric VOF that requires interface reconstruction. The other is algebraic VOF that does not require interface reconstruction. Early VOF methods are developed on structured grid. Since the topology of structured grid is regular, the geometrical operations in interface reconstruction procedure can be easily applied on structured grid. The representatives are the simple line interface calculation (SLIC)

method, which regards the interface as the horizontal or vertical lines (for 2-D) or surface (for 3-D), the PLIC (piecewise linear interface calculation)[36] method which considers the interface gradient and the preservation of mass convection. The interfaces obtained by those geometric VOF methods are accurate and sharp, but the algorithms for preserving mass conservation and interface sharpness are complex and difficult to extend to unstructured grids. The algebraic VOF methods are preferred for unstructured grid since they solve the volume fraction equation directly without interface reconstruction. Some high-resolution schemes are needed to suppress the numerical diffusion near interface and keep the volume fraction solution bounded. The compressive interface capturing scheme for arbitrary meshes (CICSAM)[37], high resolution interface capturing (HRIC)[38] and multidimensional universal limiter with explicit solution (MULES)[39] are mostly common used algebraic VOF methods in commercial or open source CFD packages. These algebraic VOF methods, however, have drawbacks and could generate unphysical results such as unbounded volume fractions when predicting complex flows. Another set of algebraic VOF schemes are the tangent of hyperbola for interface capturing (THINC) which assume a hyperbolic-tangent profile is assumed for the volume fraction within each cell containing the segment of interface[40]. The THINC method uses hyperbolic tangent function to calculate the volume fraction flux, which captures complex and twisted interfaces better. Recently, there have been some advancement of geometric VOF for unstructured meshes, such as isoAdvector[41-43], PLIC VOF[44], etc. The isoAdvector was first introduced as a general numerical interface algorithm for both structured and unstructured grids. It avoids the gradient calculations of traditional geometric VOF reconstruction. The basic idea of PLIC method is to split a single cell into 2 parts by a linearly interpolated plane to ensure accuracy when solving volume fraction transport equations.

In terms of free surface noise, some studies modelled the free surface flow in CFD, but the reflection of sound wave propagation at free surface was neglected. Ianniello et al.[45] considered the influence of the free surface for flow field, and found that there was a deviation between the acoustic prediction results and the pressure directly calculated by CFD. They believed that the neglect of the free surface reflection was an important reason for that deviation. Other studies considered the interface of free surface flow as a plane mirror when modelling the acoustic wave propagation. A mirror image method is adopted to represent the reflection effect[46-48]. In this method the free surface is modelled by considering an additional imaginary acoustic source, which works as a real source image with respect to the reflect plane.

2.2 *Cavitation modeling*

Cavitation noise needs to consider the phase change. A common solution strategy is to introduce cavitation model, known as mass transfer model. The derivation process is based on Rayleigh-Plesset equation in bubble dynamics, and the process of condensation and vaporization is expressed by adding a source term to the right of the equation[49]

$$\frac{\partial(\rho_v\alpha_v)}{\partial t}+\frac{\partial(\rho_v\alpha_v u_j)}{\partial x_j}=\dot{m}^+-\dot{m}^- \tag{1}$$

where ρ_v is the gas density, α_v is the vapour volume fraction and u_j is the velocity of vapor. The source terms m^+ and m^- represent the vaporization and condensation processes respectively. The expressions of source terms correspond to different cavitation models. For example, Schnerr-Sauer cavitation model is like:

$$\dot{m}^+=\frac{\rho_v\rho_l}{\rho}\alpha_v(1-\alpha_v)\frac{3}{R_b}\sqrt{\frac{2}{3}\frac{\max(p_v-p,0)}{\rho_l}},$$

$$\dot{m}^-=\frac{\rho_v\rho_l}{\rho}\alpha_v(1-\alpha_v)\frac{3}{R_b}\sqrt{\frac{2}{3}\frac{\max(p-p_v,0)}{\rho_l}} \tag{2}$$

where ρ_l is the density of liquid, p_v is the pressure of vapor and R_b is the radius of the cavity.

In addition, there are Merkle cavitation model, Zwart-Gerber-Belamri (Z-G-B) cavitation model, etc.[50]. Accurate information such as cavity pulsation is obtained through the cavitation model, as the basis for predicting cavitation sound field.

In terms of the effect of cavitation on sound propagation, a first-order monopole was construct as cavitation sound source[51-52], which radiates to far fields according to the spherical wave transmission law. It is written as

$$p'(r,t)=\frac{\rho\ddot{V}_c(t)}{4\pi r} \tag{3}$$

where $\ddot{V}_c$ is second-order time derivative of the cavity volume, r is the distance vector from the sound source to the test point.

This method is suitable for VOF interface cap-

turing method, because the cavity volume is easily determined from the volume fraction value of grids[51]. Although there have been some theoretical studies on the sound radiation of non-spherical cavities, a perfect solution has not yet been formed. Therefore, the main method is still to consider the cavity as a spherical sound source (see Fig. 3).

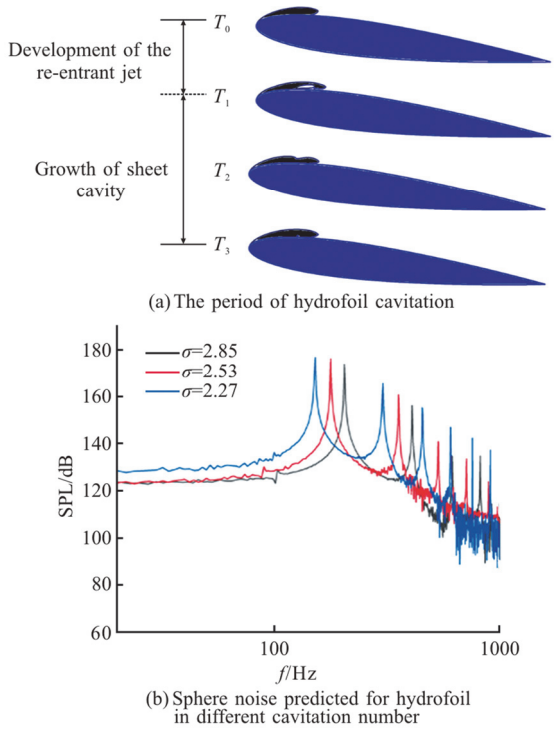

Fig. 3 (Color online) Hydrofoil cavitation noise prediction[49]

Kim et al.[51] investigated the cavitation flow around a hydrofoil and its radiated hydroacoustic field. They compared the cavitation noise predicted by different turbulence models, and found that ignoring the viscous layer would lead to distortion. Yuan et al.[53] conducted unsteady numerical simulation on a pump-jet propeller based on DES and Z-G-B cavitation model. Dubbioso et al.[52] used a spherical monopole model to calculate the cavitation noise, and applied it to propeller cavitation noise prediction in maneuvering motions. More literatures do not consider the independent influence of cavitation on acoustic sources, and believe that cavity only affects the flow field results, without additional discuss[54-55]. It is worth mentioning that the spherical source needs to use the volume integral, so it requires a large amount of calculation and accurate cavitation model.

Cavitations that do not exceed half the chord length are generally considered stable (steady cavitation), but such cavitation has extremely unstable pressure fluctuations in the closed region of the cavity[56], forming severe noise, and its frequency depends on cavity length. For unsteady cavitation, re-entrant jets and collapse are the main sound sources. As the cavitation number increases, the cavitation period becomes shorter and the sound pressure amplitude increases[49, 57]. The hydrofoil steady cavitation experiment shows that the sound peak frequency is consistent with the expansion and contraction frequency. This verifies the conclusion that cavitation dominates noise[58]. For hydrofoil unsteady cavitation, there are two pressure peaks during the cavitation process. The first peak is caused by shedding, and the second peak is induced by the collapse of large cavity into small bubbles.

2.3 *Air-water-bubble mixed flow modeling*

The premise of air-water-bubble mixed flow noise prediction is to simulate the flow accurately. At present, the numerical simulation methods of air-water-bubble mixed flow can be divided into two categories: with-interface methods and non-interface methods[59].

With-interface methods can simulate the shape changes of the two-phase interface, such as bubble shape, droplet breakup, etc.[60]. It is suitable for the simulation of the generation process of air-water-bubble mixed flow caused by bow breaking and wave rolling. If the number of bubbles in the problem is large (above 10^4), and the shape of bubbles is not concerned, the non-interface model can be used to study its evolution. It is suitable for the simulation of processes such as ship bubble sweeping down.

In addition to the VOF and level-set methods, with-interface type mainly include lattice-Boltzmann methods (LBM), particle methods, etc. Traditional CFD methods (FEM, FVM and FDM) are based on the continuum assumption. LBM starts from the discrete model and statistical mechanics, and believes that the macroscopic fluid is composed of a large number of virtual fluid particles[61]. The characteristics of fluid motion can be obtained by statistical analysis of discrete particles. It is easy to deal with the two-phase interface problem. The treatment of the phase interface problem is transformed into the control of the force between fluid particles. The “convection-collision” algebraic equation of LBM is simple in form, and there is no need to solve Possion equation. The relaxation iteration is a local operation that can be performed simultaneously, which is suitable for large-scale parallel computing.

Meshless particle method is a new numerical technology. Compared with traditional mesh methods, particle method has great flexibility in dealing with some large deformation problems[62]. Therefore, it has been widely used in bubble dynamics problems to achieve precise capture of complex phase interfaces caused by bubble deformation. Since particle method does not need to generate a mesh, there is no case that

the mesh mutation affects the flow field[63]. At the same time, it is easier to deal with the numerical simulation of the moving boundary problem because there is no need to consider the mesh deformation. However, the usability of meshless method for acoustic prediction still need to be assessed[64].

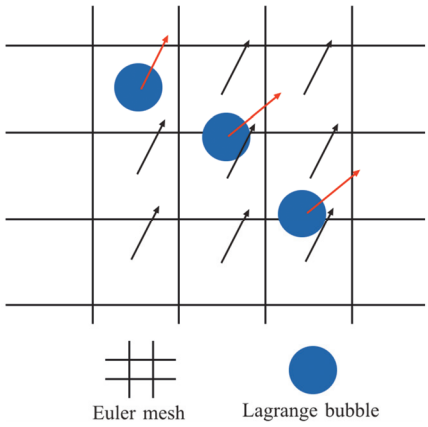

Fig. 4 (Color online) Sketch drawing of Euler-Lagrange method

Non-interface type can be divided into Euler-Lagrange methods and Euler-Euler methods. If the bubble is assumed to be a non-deformed sphere and its motion evolution is studied, Euler-Lagrange method can be used to model this flow. In this method, liquid phase and bubble phase adopt different description viewpoints: the former is solved in Euler coordinate system, and the physical quantity information at the center of the grid is obtained, see Fig. 4. The motion of the bubbles is tracked in Lagrange coordinates by the kinetic equations[65]. Collision calculations are important when modeling air-water-bubble mixed flows with high gas fractions or where bubbles interact with walls (ship hulls, etc.). In Euler-Lagrange method, the collision model can be used to simulate the multivariate elastic collision process. Since each bubble is tracked individually, it is possible to simulate mixed flow with different particle properties, such as bubbles with different diameters[66]. Furthermore, complex dynamic behaviors such as bubble breaking and coalescence can also be simulated.

Euler-Euler method considers both gas and liquid phases as continuous and assumes interpenetration between the two phases. The governing equations for the gas and liquid phases are expressed in the same form. The Euler-Euler method has a small amount of calculation and is suitable for simulating the flow with large bubble content, but cannot predict the dynamic behavior between bubbles (collision, coalescence, fragmentation, etc.)[67].

The advantages and disadvantages of various simulation methods for air-water-bubble mixed flow are compared in the following Table 1.

3. Noise reduction design

Understanding the flow structures is vital for noise reduction design. Primary vortical structures need to be identified and extracted for exploring noise reduction concepts and strategies.

3.1 *Vortex identification*

Vortex is considered to be the main origin of hydrodynamics noise. Therefore, vortex identification

Table 1 Summary of numerical simulation methods for air-water-bubble flow

Methods		Advantage	Disadvantage
With-interface type	VOF	Higher interface capture accuracy	High mesh quality requirements and complex reconstruction algorithm
	Level set	The principle is simple, easy to program and implement, and the interface geometric information (normal vector, curvature) is easy to obtain.	Prone to non-conservation of mass, limited accuracy
	LBM	The form of the governing equation is simple. The solution accuracy is high. It is good at simulating topological change of interface.	Different models need to be established for different two-phase flow, and the applicability of complex problems is limited.
	Particle method	Good at simulating severe deformation flow of free surface.	The computation const is huge, and the two-phase model is not mature yet.
Non-interface type	Euler-Lagrange method	In the simulation of a large number of bubble flow problems, the calculation cost is lower, and the interaction between bubbles can be simulated with relatively high accuracy.	The calculation cost is higher than Euler-Euler method. The force of the bubble needs to be modeled, and the simulation accuracy is affected by the model.
	Euler-Euler method	Compared with with-interface type, the calculation cost is greatly reduced, and it is good at calculating dense bubble flow.	The interfacial force model is not perfect, which can only simulate the multi-bubble flow of the same size.

is very important for gaining insight into the mechanism of noise generation and reduction. To better characterize the involved vortical structures, a good vortex identification method is necessary for in-depth analysis of complex flows.

Compared with the vorticity and other eigenvalue-based criteria like Q, λ_{ci} [68], the Liutex method is the third-generation vortex identification method recently proposed by Liu[69-71]. The Liutex method is defined by the Liutex vector $\boldsymbol{R}$, whose expression is

$$\boldsymbol{R} = R\boldsymbol{r} = \left[\boldsymbol{\omega}\cdot\boldsymbol{r} - \sqrt{(\boldsymbol{\omega}\cdot\boldsymbol{r})^2 - 4\lambda_{ci}^2}\right]\boldsymbol{r} \tag{4}$$

where R is the magnitude of the Liutex vector, $\boldsymbol{r}$ is the unit real eigenvector of the velocity gradient tensor, $\boldsymbol{\omega}$ is the vorticity vector and λ_{ci} is the imaginary part of the complex-conjugate eigenvalue.

The main feature of the Liutex method is that it extracts the pure rigid-body rotation through the decomposition of the fluid motion, thus solving the troublesome shearing contamination problem. With this unique advantage, the Liutex method can perform better in the above-mentioned wall-bounded flows and shear-dominated flows, providing convincing vortical structures for analysis. Moreover, compared with previous eigenvalue-based criteria, the Liutex method uses the vector instead of the scalar to describe the local rotation. The direction of the Liutex vector represents the direction of the local rotational axis, and the magnitude of the Liutex vector reveals the local rotational strength. In other words, the Liutex method can give more details of the flow field. For example, the formation and dissipation of vortical structures can be further characterized by the behavior of the rotational axis, obtained by integrating Liutex vectors. Using the integrated Liutex lines, Chen et al.[72] found that the rotational axis of the necklace vortex becomes spiral-like as it develops downstream, suggesting a dissipative process (shown in Fig. 5).

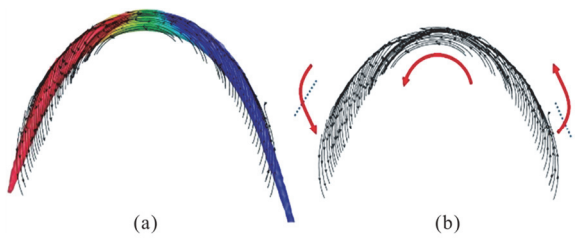

Fig. 5 (Color online) Liutex lines of necklace vortex in flow around a surface-piercing finite cylinder: (a) Liutex lines with iso-surface of $\tilde{\Omega}_R = 0.65$, colored by time-averaged vorticity and (b) Liutex lines only[72]

On the other hand, the eigenvalue-based criteria are very sensitive to the chosen threshold. As the threshold increases, the shape of the extracted vortical structure varies greatly, which poses a great challenge on how to choose an appropriate threshold for different cases. To address this issue, Dong et al.[73] proposed a normalized variant, the Omega-Liutex method Ω_R, which is defined by a normalized scalar:

$$\Omega_R = \frac{\beta^2}{\beta^2 + \alpha^2 + \varepsilon} \tag{5}$$

$$\alpha = \frac{1}{2}\sqrt{\left(\frac{\partial u_y}{\partial y} - \frac{\partial u_x}{\partial x}\right)^2 + \left(\frac{\partial u_y}{\partial x} - \frac{\partial u_x}{\partial y}\right)^2},$$

$$\beta = \frac{1}{2}\left(\frac{\partial u_y}{\partial x} - \frac{\partial u_x}{\partial y}\right) \tag{6}$$

where $\varepsilon = b_0(\beta^2 - \alpha^2)_{\max}$, b_0 is set to 10^{-6} in marine hydrodynamics, according to a sensitive study[74]. On this basis, Liu and Liu[75] subsequently improved the original method and proposed a modified Omega-Liutex method $\tilde{\Omega}_R$ to resolve the bulging phenomenon, as shown in Fig. 6. The normalized scalar then becomes

$$\tilde{\Omega}_R = \frac{\beta^2}{\beta^2 + \alpha^2 + \lambda_{cr}^2 + 1/2\lambda_r^2 + \varepsilon} \tag{7}$$

where λ_{cr} is the real part of the complex-conjugate eigenvalues, λ_r is the real eigenvalue

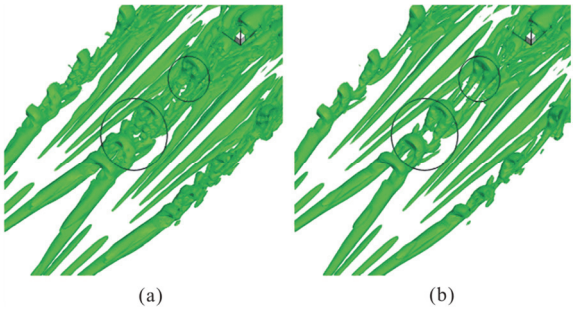

Fig. 6 (Color online) Iso-surface of hairpin vortex structures in boundary layer transition on a flat plate[70]

For these normalized methods, the extracted vortical structures is almost independent of the threshold and the threshold of iso-surfaces is recommended to be 0.52, which can capture both strong and weak vortices simultaneously. In this way, the weak vortices in the far-field wake, which usually

correspond to the far-field noise, can be well preserved together with the strong vortices near the structure. Zhao et al.[74] applied the modified Omega-Liutex method to the propeller wake using different thresholds, as shown in Fig. 7. The comparison shows that the primary vortical structure behind the blade, the tip vortex, does not change substantially with the threshold.

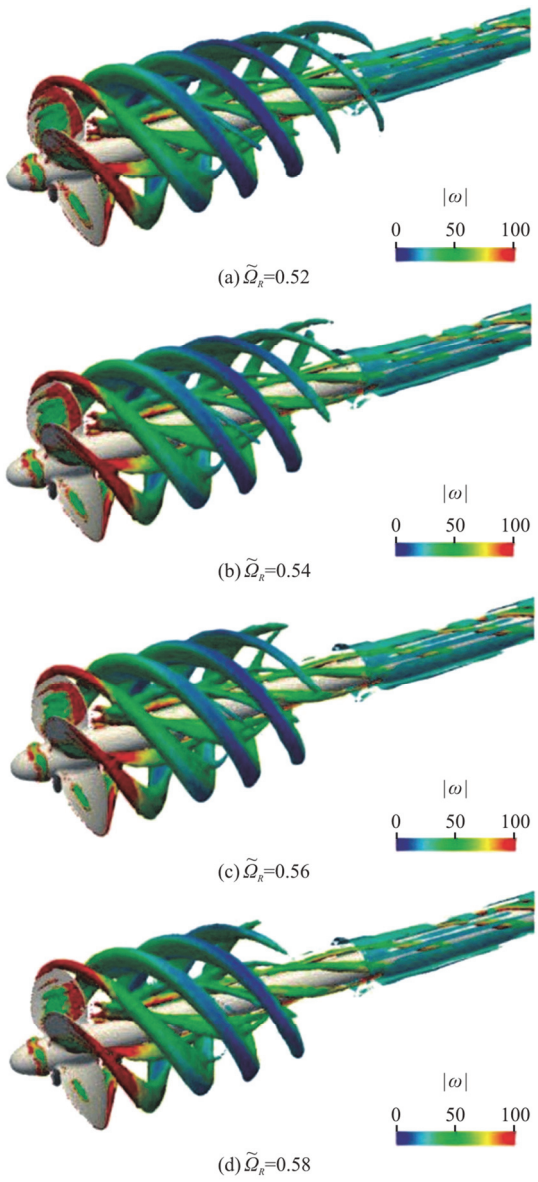

Fig. 7 (Color online) Iso-surfaces of vortical structures in propeller wake using Ω_R [74]

3.2 *Noise control*

One of the most significant low-noise design is the problem of cavitation noise suppression in engineering. The suppression of cavitation noise can be divided into two methods: active control and passive control[76].

Active control is implemented by injecting air or water at the leading edge of the hydrofoil or the tip of the propeller blade generally. Studies found that setting the water injection holes at the leading edge of the hydrofoil can improve the severe pressure fluctuation and reduce the intensity of dipole and quadrupole significantly. The reason is that the injected water provides additional energy to the flow field, delaying the boundary layer separation[77]. Similarly, setting air outlets can also improve surface pressure fluctuations significantly[78]. It is found in full-scale observations that propeller cavitation often occurs at the blade tip (tip vortex cavitation) first, and then the noise level increases sharply[79]. Water injection at the tip can delay the occurrence of tip vortex cavitation significantly, thereby reducing cavitation noise[80]. Figure 8 is a schematic diagram of active suppression of cavitation noise by hydrofoil and propeller respectively. The injected flow can be easily implemented in the CFD simulation by setting inflow condition at the holes on the surface.

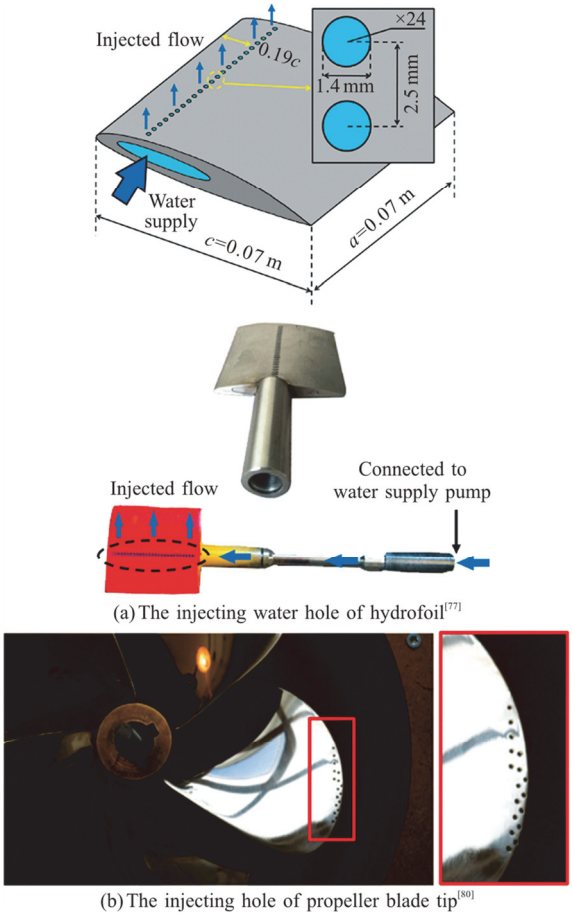

Fig. 8 (Color online) Low-noise structure design

Passive control refers to changing the structure of hydrofoil or propeller, so as to achieve the purpose of reducing cavitation noise. Highly skewed propellers induce lower cavitation noise generally[81]. Ku et al.[33]

studied the cavitation noise of SUBOFF submarine propellers, and confirmed that highly skewed propellers reduce cavitation noise. Cavitation noise can be suppressed by setting small slots on the object surface[82]. Dang et al.[83] opened micro-slots on the hydrofoil spanwise and found that high-frequency noise can be reduced. Huang et al.[84-85] found that both C-shaped slots and T-shaped slots suppress hydrofoil cavitation noise effectively. In addition, changing the trailing edge into a sawtooth structure can also reduce cavitation noise[86]. This type of wavy structure is also effective on the leading edge of the propeller blade. It has also been found that increasing the surface roughness of the propeller reduces the cavity volume and cavitation noise, although it will sacrifice part of the propulsion efficiency[87]. The mechanism of the effect of surface roughness on cavitation noise is not yet clear, and it is believed that it affects the development of the boundary layer mainly.

4. Conclusions and outlook

Hydrodynamic flows often involve turbulence, boundary layer transition, flow separation, complex geometries, moving boundaries, free surface flows, cavitation flows, air-water-bubble mixing flows, etc. To predict the hydrodynamic noise accurately requires the fundamental understanding of the complex physical process of the flows. Proper numerical models should be selected to reproduce the core characteristics of the physical phenomena.

In the foreseen future, the hybrid methods will be the main approach for studying hydrodynamic noise for engineering flows. The unsteady properties of flow affect the sound generation directly and are an important part of noise prediction. Currently the lack of high-quality experimental data for unsteady flow and noise is the main obstacle for the validation of newly developed numerical methods. Hybrid use of the computational and experimental tools will be a promising way to explore new low-noise designs.

Compliance with Ethical Standards

Conflict of Interest: The authors declare that they have no conflict of interest.

Ethical approval: This article does not contain any studies with human participants or animals performed by any of the authors.

Informed consent: Informed consent was obtained from all individual participants included in the study.

References

[1] Suresh T., Szulc O., Flaszynski P. et al. Prediction of helicopter rotor noise in hover using FW-H analogy [J]. *Journal of Physics: Conference Series*, 2018, 1101(1): 012041.

[2] Spalart P. R., Belyaev K. V., Shur M. L. et al. On the differences in noise predictions based on solid and permeable surface Ffowcs Williams–Hawkings integral solutions [J]. *International Journal of Aeroacoustics*, 2019, 18(6-7): 621-646.

[3] Turner J. M., Kim J. W. Effect of spanwise domain size on direct numerical simulations of airfoil noise during flow separation and stall [J]. *Physics of Fluids*, 2020, 32(6): 065103.

[4] Choi W. S., Choi Y., Hong S. Y. et al. Turbulence-induced noise of a submerged cylinder using a permeable FW–H method[J]. *International Journal of Naval Architecture and Ocean Engineering*, 2016, 8(3): 235-242.

[5] Posa A., Felli M., Broglia R. Influence of an upstream hydrofoil on the acoustic signature of a propeller [J]. *Physics of Fluids*, 2022, 34(4): 045112.

[6] Slotnick J. P., Khodadoust A., Alonso J. et al. CFD vision 2030 study: A path to revolutionary computational aerosciences [R]. NF1676L-18332, 2014.

[7] Larsson J., Kawai S., Bodart J. et al. Large eddy simulation with modeled wall-stress: Recent progress and future directions [J]. *Mechanical Engineering Reviews*, 2016, 3(1): 1-23.

[8] Suga K., Sakamoto T., Kuwata Y. Algebraic non-equilibrium wall-stress modeling for large eddy simulation based on analytical integration of the thin boundary-layer equation [J]. *Physics of Fluids*, 2019, 31(7): 075109.

[9] Lozano-Durán A., Giometto M. G., Park G. I. et al. Non-equilibrium three-dimensional boundary layers at moderate Reynolds numbers [J]. *Journal of Fluid Mechanics*. 2020, 883: A20.

[10] Iyer P. S., Malik M. R. Analysis of the equilibrium wall model for high-speed turbulent flows [J]. *Physical Review Fluids*, 2019, 4(7): 074604.

[11] Mehrabadi M., Bodony D. J. Wall-modeled large-eddy simulation and direct numerical simulation of broadband trailing edge noise from a NACA 0012 airfoil [C]. *25th AIAA/CEAS Aeroacoustics Conference*, Delft, The Netherlands, 2019.

[12] Boukharfane R., Parsani M., Bodart J. Characterization of pressure fluctuations within a controlled-diffusion blade boundary layer using the equilibrium wall-modelled LES [J]. *Scientific Reports*, 2020, 10(1): 12735.

[13] Posa A., Broglia R., Felli M. et al. Hydroacoustic analysis of a marine propeller using large-eddy simulation and acoustic analogy [J]. *Journal of Fluid Mechanics*, 2022, 947: A46.

[14] Shu C. W. Essentially non-oscillatory and weighted essentially non-oscillatory schemes [J]. *Acta Numerica*, 2020, 29: 701-762.

[15] Brus S. R., Wirasaet D., Kubatko E. J. et al. High-order discontinuous Galerkin methods for coastal hydrodynamics applications [J]. *Computer Methods in Applied Mechanics and Engineering*, 2019, 355: 860-899.

[16] Huismann I., Stiller J., Fröhlich J. Efficient high-order spectral element discretizations for building block operators of CFD [J]. *Computers and Fluids*, 2020, 197: 104386.

[17] Vincent P. E., Farrington A. M., Witherden F. D. et al. An extended range of stable-symmetric-conservative Flux Reconstruction correction functions [J]. *Computer Methods in Applied Mechanics and Engineering*, 2015, 296: 248-272.

[18] Hu Y. S., Zhang P. J. Y., Wan Z. H. et al. Effects of

trailing-edge serration shape on airfoil noise reduction with zero incidence angle [J]. *Physics of Fluids*, 2022, 34(10): 105108.
[19] Marino O. A., Ferrer E., Valero E., et al. Aeroacoustic simulations of 3D airfoil sections using a high order discontinuous Galerkin solver [C]. *AIAA SCITECH 2022 Forum*, San Diego, California, USA, 2021.
[20] Alhawwary M. A., Wang Z. J. Implementation of a FWH approach in a high-order LES tool for aeroacoustic noise predictions [C]. *AIAA Scitech 2020 Forum*, Orlando, Florida, USA, 2020.
[21] Shen W., Miller S. A. E. Validation of a high-order large eddy simulation solver for acoustic prediction of supersonic jet flow [J]. *Journal of Theoretical and Computational Acoustics*, 2020, 28(3): 1950023.
[22] Ren Z., Wang J., Wan D. Investigation of fine viscous flow fields in ship planar motion mechanism tests by DDES and RANS methods [J]. *Ocean Engineering*, 2022, 243: 110272.
[23] Carrica P. M., Mofidi A., Eloot K. et al. Direct simulation and experimental study of zigzag maneuver of KCS in shallow water [J]. *Ocean Engineering*, 2016, 112: 117-133.
[24] Shen Z., Ye H., Wan D. URANS simulations of ship motion responses in long-crest irregular waves [J]. *Journal of Hydrodynamics*, 2014, 26(3): 436-446.
[25] Shen Z., Wan D. RANS computations of added resistance and motions of a ship in head waves [J]. *International Journal of Offshore and Polar Engineering*, 2013, 23(4): 263-271.
[26] Shen Z., Wan D., Carrica P. M. Dynamic overset grids in OpenFOAM with application to KCS self-propulsion and maneuvering [J]. *Ocean Engineering*, 2015, 108: 287-306.
[27] Noack R., Boger D., Kunz R. F. et al. Suggar++: An improved general overset grid assembly capability [C]. *19th AIAA Computational Fluid Dynamics*. San Antonio, Texas, USA, 2009.
[28] Wang J., Zou L., Wan D. Numerical simulations of zigzag maneuver of free running ship in waves by RANS-Overset grid method [J]. *Ocean Engineering*. 2018, 162: 55-79.
[29] Wang J., Wan D. Application progress of computational fluid dynamic techniques for complex viscous flows in ship and ocean engineering [J]. *Journal of Marine Science and Application*, 2020, 19(1): 1-16.
[30] Sezen S., Cosgun T., Yurtseven A. et al. Numerical investigation of marine propeller underwater radiated noise using acoustic analogy Part 1: The influence of grid resolution [J]. *Ocean Engineering*, 2021, 220: 108448.
[31] Wang Z., Li L., Cheng H. et al. Numerical investigation of unsteady cloud cavitating flow around the Clark-Y hydrofoil with adaptive mesh refinement using OpenFOAM [J]. *Ocean Engineering*, 2020, 206: 107349.
[32] Lidtke A. K., Lloyd T., Lafeber F. H. et al. Predicting cavitating propeller noise in off-design conditions using scale-resolving CFD simulations [J]. *Ocean Engineering*, 2022, 254: 111176.
[33] Ku G., Cho J., Cheong C. et al. Numerical investigation of tip-vortex cavitation noise of submarine propellers using hybrid computational hydro-acoustic approach [J]. *Ocean Engineering*, 2021, 238: 109693.
[34] Sezen S., Atlar M. Marine propeller underwater radiated noise prediction with the FWH acoustic analogy Part 3: Assessment of full-scale propeller hydroacoustic performance versus sea trial data [J]. *Ocean Engineering*, 2022, 266: 112712.
[35] Scapin N., Costa P., Brandt L. A volume-of-fluid method for interface-resolved simulations of phase-changing two-fluid flows [J]. *Journal of Computational Physics*, 2020, 407: 109251.
[36] Nahed J., Dgheim J. Estimation curvature in PLIC-VOF method for interface advection [J]. *Heat and Mass Transfer*, 2020, 56(3): 773-787.
[37] Li L. M., Hu D. Q., Liu Y. C. et al. Large eddy simulation of cavitating flows with dynamic adaptive mesh refinement using OpenFOAM [J]. *Journal of Hydrodynamics*, 2019, 32(2): 398-409.
[38] Najafi A., Nowruzi H. On hydrodynamic analysis of stepped planing crafts [J]. *Journal of Ocean Engineering and Science*, 2019, 4(3): 238–251.
[39] Choi Y. M., Kim Y. J., Bouscasse B. et al. Performance of different techniques of generation and absorption of free-surface waves in computational fluid dynamics [J]. *Ocean Engineering*, 2020, 214: 107575.
[40] Deng X., Inaba S., Xie B. et al. High fidelity discontinuity-resolving reconstruction for compressible multiphase flows with moving interfaces [J]. *Journal of Computational Physics*, 2018, 371: 945-966.
[41] Roenby J., Bredmose H., Jasak H. A computational method for sharp interface advection [J]. *Royal Society Open Science*, 2016, 3(11): 160405.
[42] Scheufler H., Roenby J. Accurate and efficient surface reconstruction from volume fraction data on general meshes [J]. *Journal of Computational Physics*, 2019, 383: 1-23.
[43] Gamet L., Scala M., Roenby J. et al. Validation of volume-of-fluid OpenFOAM® isoAdvector solvers using single bubble benchmarks [J]. *Computers and Fluids*, 2020, 213: 104722.
[44] Chen S., Zhao W., Wan D. Turbulent structures and characteristics of flows past a vertical surface-piercing finite circular cylinder [J]. *Physics of Fluids*, 2022, 34(1): 015115.
[45] Ianniello S., Muscari R., Di Mascio A. Ship underwater noise assessment by the acoustic analogy Part II: hydroacoustic analysis of a ship scaled model [J]. *Journal of Marine Science and Technology*, 2014, 19(1): 52-74.
[46] Cianferra M., Armenio V. Scaling properties of the Ffowcs-Williams and Hawkings equation for complex acoustic source close to a free surface [J]. *Journal of Fluid Mechanics*, 2021, 927: A2.
[47] Bosschers J. Propeller tip-vortex cavitation and its broadband noise [D]. Doctoral Thesis, Enschede, The Netherlands: University of Twente, 2018.
[48] Bosschers J. A semi-empirical prediction method for broadband hull-pressure fluctuations and underwater radiated noise by propeller tip vortex cavitation [J]. *Journal of Marine Science and Engineering*, 2018, 6(2): 49.
[49] Yu L., Zhao W., Wan D. et al. Nonlinear noise of hydrofoil cavitation considering sound velocity variation and phase transitions [J]. *Ocean Engineering*, 2022, 264: 112506.
[50] Yu L. J., Wu J. W., Wan D. C. Correlation analysis between underwater noise and Liutex for DTMB4119 propeller [J]. *Journal of Hydrodynamics*, 2022, 34(4): 585-595.
[51] Kim S., Cheong C., Park W. G. Numerical investigation into effects of viscous flux vectors on hydrofoil cavitation flow and its radiated flow noise [J]. *Applied Sciences*, 2018, 8(2): 289.
[52] Dubbioso G., Muscari R., Ortolani F. et al. Numerical analysis of marine propellers low frequency noise during

maneuvering [J]. *Applied Ocean Research*, 2021, 106: 102461.
[53] Yuan J., Chen Y., Wang L. et al. Dynamic analysis of cavitation tip vortex of pump-jet propeller based on DES [J]. *Applied Sciences*, 2020, 10(17): 5998.
[54] Lidtke A. K., Humphrey V. F., Turnock S. R. Feasibility study into a computational approach for marine propeller noise and cavitation modeling [J]. *Ocean Engineering*, 2016, 120: 152-159.
[55] Testa C., Ianniello S., Salvatore F. A Ffowcs Williams and Hawkings formulation for hydroacoustic analysis of propeller sheet cavitation [J]. *Journal of Sound and Vibration*, 2018, 413: 421-441.
[56] Zhao M., Wan D., Gao Y. Comparative study of different turbulence models for cavitational flows around NACA0012 hydrofoil [J]. *Journal of Marine Science and Engineering*, 2021, 9(7): 742.
[57] Yu A., Wang X., Zou Z. et al. Investigation of cavitation noise in cavitating flows around an NACA0015 hydrofoil [J]. *Applied Sciences*, 2019, 9(18): 3736.
[58] Ahn B. K., Jeong S. W., Park C. S. et al. An experimental investigation of coherent structures and induced noise characteristics of the partial cavitating flow on a two-dimensional hydrofoil [J]. *Fluids*, 2020, 5(4): 198.
[59] Li Z., Zhang X. S., Wan D. C. Research progress on the hydrodynamic performance of water-air-bubble mixed flows around a ship [J]. *Journal of Hydrodynamics*. 2022, 34(2): 171-188.
[60] Wu D., Wang J., Wan D. Delayed detached eddy simulation method for breaking bow waves of a surface combatant model with different trim angle [J]. *Ocean Engineering*, 2021, 242: 110177.
[61] Petersen K. J., Brinkerhoff J. R. On the lattice Boltzmann method and its application to turbulent, multiphase flows of various fluids including cryogens: A review [J]. *Physics of Fluids*, 2021, 33(4): 041302.
[62] Huang C., Zhang G., Wan D. Hydroelastic responses of an elastic cylinder impacting on the free surface by MPS-FEM coupled method [J]. *Acta Mechanica Sinica*, 2022, 38(11): 322057.
[63] Xie F., Meng Q., Wan D. Numerical simulations of liquid-solid flows in a vertical pipe by MPS-DEM coupling method [J]. *China Ocean Engineering*, 2022, 36(4): 542-552.
[64] You X., Li W., Chai Y. A truly meshfree method for solving acoustic problems using local weak form and radial basis functions [J]. *Applied Mathematics and Computation*, 2020, 365: 124694.
[65] Zhang X., Zhao W., Wan D. A hybrid volume-of-fluid/ Euler–Lagrange method for vertical plunging jet flows [J]. *International Journal of Offshore and Polar Engineering*, 2022, 32(1): 31-38.
[66] Zhang X., Wang J., Wan D. An improved multi-scale two phase method for bubbly flows [J]. *International Journal of Multiphase Flow*, 2020, 133: 103460.
[67] Hu Y. D., Wu J. W., Wan D. C. et al. Preliminary control of the air entrainment in bow wave based on the Liutex force method [J]. *Journal of Hydrodynamics*, 2022, 34(3): 483-490.
[68] Zhang Y. N., Qiu X., Chen F. P. et al. A selected review of vortex identification methods with applications [J]. *Journal of Hydrodynamics*, 2018, 30(5): 767-779.
[69] Gao Y., Liu C. Rortex based velocity gradient tensor decomposition [J]. *Physics of Fluids*, 2019, 31(1): 011704.
[70] Gao Y., Liu C. Rortex and comparison with eigenvalue-based vortex identification criteria [J]. *Physics of Fluids*, 2018, 30(8): 085107.
[71] Liu C., Gao Y., Tian S. et al. Rortex–A new vortex vector definition and vorticity tensor and vector decompositions [J]. *Physics of Fluids*, 2018, 30(3): 035103.
[72] Chen S., Zhao W., Wan D. Turbulent structures and characteristics of flows past a vertical surface-piercing finite circular cylinder [J]. *Physics of Fluids*, 2022, 34(1): 015115.
[73] Dong X., Gao Y., Liu C. New normalized Rortex/vortex identification method [J]. *Physics of Fluids*, 2019, 31(1): 011701.
[74] Zhao W. W., Wang J. H., Wan D. C. Vortex identification methods in marine hydrodynamics [J]. *Journal of Hydrodynamics*, 2020, 32(2): 286-295.
[75] Liu J., Liu C. Modified normalized Rortex/vortex identification method [J]. *Physics of Fluids*, 2019, 31(6): 061704.
[76] Yu L. J., Zhao W. W., Wan D. C. Research progress and application of computational method for hydrodynamic noise from air-water interface [J]. *Chinese Journal of Ship Research*, 2022, 17(5): 85-102.
[77] Wang W., Li Z., Liu M. et al. Influence of water injection on broadband noise and hydrodynamic performance for a NACA66 (MOD) hydrofoil under cloud cavitation condition [J]. *Applied Ocean Research*, 2021, 115: 102858.
[78] Sun T., Wang Z., Zou L. et al. Numerical investigation of positive effects of ventilated cavitation around a NACA66 hydrofoil [J]. *Ocean Engineering*, 2020, 197: 106831.
[79] Lee C. S., Ahn B. K., Han J. M. et al. Propeller tip vortex cavitation control and induced noise suppression by water injection [J]. *Journal of Marine Science and Technology*, 2018, 23(3): 453-463.
[80] Aktas B., Yilmaz N., Atlar M. et al. Suppression of tip vortex cavitation noise of propellers using PressurePoresTM technology [J]. *Journal of Marine Science and Engineering*, 2020, 8(3): 158.
[81] Asnaghi A., Svennberg U., Bensow R. E. Numerical and experimental analysis of cavitation inception behaviour for high-skewed low-noise propellers [J]. *Applied Ocean Research*, 2018, 79: 197-214.
[82] Liu C., Yan Q., Wood H. G. Numerical investigation of passive cavitation control using a slot on a three-dimensional hydrofoil [J]. *International Journal of Numerical Methods for Heat and Fluid Flow*, 2019, 30(7): 3585-3605.
[83] Dang Z., Mao Z., Tian W. Reduction of hydrodynamic noise of 3D hydrofoil with spanwise microgrooved surfaces inspired by sharkskin [J]. *Journal of Marine Science and Engineering*, 2019, 7(5): 136.
[84] Huang Z., Han Y., Tan L. et al. Influence of T-shape tip clearance on energy performance and broadband noise for a NACA0009 hydrofoil [J]. *Energies*, 2019, 12(21): 4066.
[85] Huang Z., Huang Z., Fan H. Influence of C groove on energy performance and noise source of a NACA0009 hydrofoil with tip clearance [J]. *Renewable Energy*, 2020, 159: 726-735.
[86] Arce León C., Ragni D., Pröbsting S. et al. Flow topology and acoustic emissions of trailing edge serrations at incidence [J]. *Experiments in Fluids*, 2016, 57(5): 91.
[87] Sezen S., Uzun D., Ozyurt R., et al. Effect of biofouling roughness on a marine propeller's performance including cavitation and underwater radiated noise (URN) [J]. *Applied Ocean Research*, 2021, 107: 102491.